Article

pubs.acs.org/Biomac

Small Angle Neutron Scattering Studies on the Internal Structure of Poly(lactide-*co*-glycolide)-*block*-poly(ethylene glycol) Nanoparticles as Drug Delivery Vehicles

Bin Yang,[†,§] John P. Lowe,[†] Ralf Schweins,[‡] and Karen J. Edler*[,†]

[†]Department of Chemistry, University of Bath, Claverton Down, Bath, BA2 7AY, U.K.

[‡]Large Scale Structures Group, Institut Laue-Langevin, 71 Avenue des Martyrs, CS 20156, F-38042 CEDEX 9 Grenoble, France

Supporting Information

ABSTRACT: Poly(lactide-*co*-glycolide)-*block*-poly(ethylene glycol) (PLGA-PEG) nanoparticles are commonly used as drug carriers in controlled drug release and targeting. To achieve predictable and clinically relevant volumes of drug distribution, nanoparticle size, surface charge, and especially composition and structure must be controlled. Understanding the internal structures within the particles is fundamentally important to explain differences in drug loading and variations in drug release rate. We prepared nanoparticles from ester-terminated PLGA-PEG polymers via nanoprecipitation, and studied the effects of altering the solvent−water miscibility (THF, acetone, and acetonitrile). Morphology, size, polydispersity, and ζ-potential of PLGA-PEG nanoparticles were characterized. Small angle neutron scattering measurements and fitted models revealed the internal nanoparticle structure: PLGA blocks of 7−9 nm are encapsulated inside a fairly dense PEG/water network in a fractal geometry. Particles with a larger PLGA block volume and higher PEG volume fraction in the particle interior result in greater retention of the hydrophilic anticancer drug carboplatin.

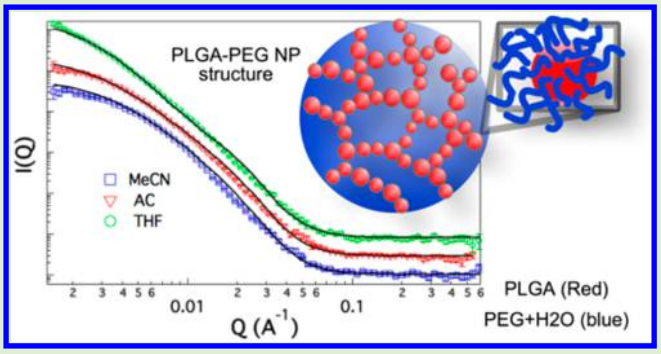

1. INTRODUCTION

Poly(lactic-*co*-glycolic acid) PLGA nanoparticles have attracted considerable attention due to their attractive properties such as biodegradability, biocompatibility, well described formulations, controllable particle diameters, and the possibility of sustained release. Therefore, they have been chosen as drug delivery vehicles in various biomedical applications, such as cancer treatment.[1−3]

Poly(ethylene glycol) PEG is usually chosen as a hydrophilic block to provide a hydrated steric barrier, which not only can stabilize the particle but also can prolong the blood circulation time.[4,5] For example, PLGA-PEG nanoparticles loaded with cisplatin showed prolonged cisplatin residence in systemic circulation.[6] In addition, these particles were shown to enter prostate cancer cells and exerted in vitro anticancer activity that was comparable to the activity of free cisplatin.[7] Another advantage of pegylated PLGA polymer nanoparticles is that modification of the tip of the PEG strands with specific targeting receptors can allow particles to access the brain from the bloodstream via receptor mediated transcytosis and deliver the content into the brain parenchyma without damage to the blood−brain barrier (BBB).[8−10]

So far, little has been reported about the physiochemical characteristics of the pegylated PLGA or poly(lactic acid) (PLA) nanoparticles that influence their release behavior. It is possible to control the aggregation behavior of block copolymers by varying the molecular weight ratios of the hydrophobic and hydrophilic blocks.[11−13] PLA-PEG block copolymers with low molecular weight and a relatively high proportion of PEG blocks, such as $PLA_{400}PEG_{1800}$, have been shown not to form micelles in aqueous solution.[14] However, polymeric micelle-like nanoparticles can be produced from PLA-PEG diblock copolymers with a PLA portion of varying molecular weight (2−110 kDa) and PEG portion of 2−5 kDa, using simple particle preparation methods, such as emulsification or precipitation from water miscible organic solvents.[11,15,16] Previous work on PLGA/PLA-PEG nanoparticles has described them as having a core−shell micelle-like structure, which contains a PLA/PLGA core surrounded by a hydrophilic PEG corona or outer shell, with particle size solely dependent on the number of monomeric units in the PLA block. ^{1}H NMR studies indicated negligible penetration of the PEG into the solid-like PLA core for nanoparticles prepared with $PLA_{2-75kDa}PEG_{5kDa}$; however, as much of 25% of the PEG chains are trapped within the PLA core in the case of $PLA_{110kDa}PEG_{5kDa}$.[11] At room temperature, a solid-like central core and more mobile interfacial region coexist within the PLA

Received: October 14, 2014
Revised: December 21, 2014
Published: December 23, 2014

 © 2014 American Chemical Society

DOI: 10.1021/bm501519u
Biomacromolecules 2015, 16, 457−464

core of the nanoparticles, whereas the PEG corona layer on the nanoparticle surface is in the liquid state.[17]

A variety of techniques have been used to study the polymeric nanoparticles, such as light scattering and nuclear magnetic resonance; however, many of these techniques only provide information about the whole assembled structure. Small angle neutron scattering (SANS) was first used to study the internal structure of small PLA-PEG nanoparticles, prepared using nanoprecipitation by Riley et al.[18] Three different solvent contrasts were analyzed simultaneously using core−shell models, which simply concentrated on the form factor. The interparticle structure factor was disregarded due to the very low concentration of particles. This model assumes a homogeneous core with a uniform scattering length density, while the scattering density of PEG shell was described by a nonuniform scattering length density, composed mostly of polymer near the core but becoming equal to the solvent at the edge of the shell. The results suggested that the mean core dimension increased with the molecular weight of the PLA block. The thickness, structure, and density of the PEG layer were also found to depend on the molecular weight of the PLA block.

Understanding the internal structure of the polymeric nanoparticles and how it varies with particle preparation is fundamentally important to explain drug loading and drug release properties.[4] In this study, we have prepared nanoparticles from PLGA-PEG block copolymers, made by a nanoprecipitation method using three different water-soluble organic solvents. The physicochemical properties of the nanoparticles with regards to the morphology, size, polydispersity, and ζ-potential have been characterized. SANS has been used to provide direct structural information about the detailed internal structure of PLGA-PEG nanoparticles via solvent contrast variation. Differences in the carboplatin loading and in vitro release behavior will be discussed and compared with the measured internal structures.

2. EXPERIMENTAL SECTION

2.1. Materials. Poly(lactide-*co*-glycolic acid) (50:50) with terminal carboxylate groups (RG502H, MW reported by Sigma-Aldrich is 7−17 kDa, measured by GPC during this work MW ≈ 14 kDa), acetone (AC), acetonitrile (MeCN), tetrahydrofuran (THF), dichloromethane (DCM), methanol, ethyl ether, 1-ethyl-3-(3-dimethylaminopropyl) carbodiimide (EDC), *N*,*N*-diisopropylethylamine (DIEA), and *N*-hydroxysuccinimide (NHS) were purchased from Sigma-Aldrich; NH_2-PEG-CH_3 (MW ≈ 5.5 kDa) was obtained from Polymer Source Inc. (Dorval, Canada), and 10 mg/mL carboplatin solution was purchased from Accord Healthcare Limited. Artificial cerebrospinal fluid (ACSF) was purchased from R&D systems Europe Ltd.; all reagents were analytical grade or above and used as received, unless otherwise stated.

2.2. Methods. *2.2.1. Synthesis of PLGA-PEG Block Copolymer.* Ester-ended block copolymer PLGA-PEG was synthesized by conjugating NH_2-PEG-CH_3 to PLGA-COOH according to a previously described method.[8,10] The copolymer was dissolved in $CDCl_3$ and its chemical composition was characterized by ^{1}H NMR (Bruker 300 MHz), as shown in Supporting Information Figure 1; the characteristic peaks of the -CH_3, -CH_2, and -CH protons of PLGA were at 1.6, 4.8, and 5.2 ppm, respectively (as marked on the graph). The peak at 3.7 ppm belongs to the -CH_2 protons of the PEG chain. The average molecular weight was determined by gel permeation chromatography (GPC, Polymer Laboratories PL-GPC 50 integrated system). Samples were dissolved in analytical-reagent-grade tetrahydrofuran (THF); the number average and weight average molecular weights of the polymers were determined by universal calibration obtained from a polystyrene reference.

2.2.2. Preparation of PLGA and PLGA-PEG Nanoparticles. The nanoprecipitation method was employed to prepare PLGA (RG502H) or PLGA-PEG nanoparticles. Briefly, 60 mg of block copolymer was dissolved in 6 mL of an organic solvent that is miscible with water. Nanoparticles were formed by adding the polymer solution drop by drop to 18 mL of pure water under moderate magnetic stirring. The resulting nanoparticle suspension was stirred uncovered overnight at room temperature, allowing for the complete removal of the organic solvent and hardening of the particles. Anticancer drug carboplatin was encapsulated inside the particle by mixing the 1.4 mL carboplatin solution (10 mg/mL) with the polymer solution before dropwise addition to water. The nanoparticles were prepared via the nanoprecipitation method using three solvents: AC, MeCN, and THF.

For SANS experiments, the nanoparticles were prepared using the nanoprecipitation method as mentioned above directly into the D_2O/H_2O mixtures containing two different proportions of D_2O: 100% D_2O ($100D_2O$) and 70% D_2O ($70D_2O/30H_2O$). The organic-solvent-free nanoparticles suspended in the deuterated solvents were used directly for the SANS experiments.

2.2.3. Transmission Electron Microscopy (TEM). Morphological evaluation of the PLGA-PEG nanoparticles was performed using TEM (JEOL JEM 1200 EXII). A drop of NP suspension was placed on a Formvar poly(vinylformal)/carbon supported 400 mesh grid, excess liquid was removed with a filter paper, and the grid was dried in air at room temperature followed by negative staining with phosphotungstic acid solution (3% W/V). TEM images were calibrated using SIRA gratings 2160 (462 nm) lines per millimeter and catalase crystals for high magnification (8.75/6.85 nm spacing in the unit cell).

The size distributions of the PLGA-PEG nanoparticles were obtained from the TEM images using ImageJ software where at least 200 nanoparticles per sample were measured for each data set.

2.2.3. Dynamic Light Scattering. Freeze-dried nanoparticles were completely resuspended in aqueous solution by sonication in an ultrasonic bath (Fisherbrand FB 11020) for 15 min. A Zetasizer nano ZS from Malvern Instruments using light from a He-Ne laser source (λ = 633 nm) was used for dynamic light scattering measurements to generate information on particle size and polydispersity. All experiments were performed at 25 °C at a scattering angle of 173° to the incident beam, with an assumed refractive index of 1.59[19] and viscosity of 0.89 mPa·s. The average hydrodynamic particle size and polydispersity were obtained using the particle diffusion coefficient (Cumulants analysis) and Stokes−Einstein equation. Since the particles have a narrow polydispersity, the single exponential function was found to give reasonable fits for the DLS data. The intensity-weighted mean value presented is the mean of three measurements. ζ-Potential was also determined with the Zetasizer nano ZS. By measuring the electrophoretic mobility, the ζ-potential can be calculated using the Henry equation within the Smoluchowsky approximation.[20,21]

2.2.4. Small Angle Neutron Scattering. SANS data were collected on both on D11 at the ILL in Grenoble, France,[22,23] and on the SANS2D time-of-flight small angle neutron scattering instrument at ISIS spallation neutron source (Rutherford Appleton Laboratory, Didcot, UK).[24,25] The samples were placed in 1 mm thick quartz cells at room temperature. On SANS2D, sample−detector distances of 4 and 12 m were used with neutron wavelengths between 1.5 and 14 Å to provide a simultaneous Q-range of 0.002−0.074 Å^{-1}, while on D11 sample−detector distances of 1.2, 8, and 39 m were used with a neutron wavelength of 6 Å and with 13 Å at 39 m as an additional setting, to provide a Q-range of 0.0008−0.5 Å^{-1}. Q is the modulus of the scattering vector:

$$Q = \left(\frac{4\pi}{\lambda}\right)\sin\left(\frac{\theta}{2}\right) \quad (1)$$

where λ is the neutron wavelength and θ is scattering angle. All the scattering curves have been corrected for instrumental factors, normalized against a standard to absolute intensities in cm^{-1}, and a

DOI: 10.1021/bm501519u
Biomacromolecules 2015, 16, 457−464

suitable solvent background has been subtracted. Analysis of the experimental data was done using the NIST SANS analysis package[26] within Igor Pro (Wavemetrics).

The total neutron scattering intensity, $I(Q)$, from a dilute suspension of particles can be described as

$$I(Q) = \phi V_p(\Delta\rho)^2 P(Q)S(Q) + \text{bkg} \quad (2)$$

where $\Delta\rho$ is the difference (or contrast) between the neutron scattering length densities of the particle and the dispersion medium, V_p is the particle volume, ϕ is the particle volume fraction, $P(Q)$ is the intraparticle interference for a single particle, called the form factor, $S(Q)$ is the structure factor, describing the interference of scattering from different particles and containing information on the interaction between the particles, and bkg is the background.

In the SANS experiment, PLGA-PEG nanoparticles were directly prepared in D_2O/H_2O mixtures containing two different proportions of D_2O, 100% D_2O and 70% D_2O, in order to avoid the uncertainties in the solvent composition, which could arise from carrying out a solvent exchange after particle preparation. Data from the solutions with two different D_2O contents was fitted simultaneously. In this approach, the parameters for a particular data set should be identical to those for the particles in the solution at the other D_2O content except for the change in SLD values. Hence, this is expected to yield more representative structural parameters than would be the case if the data sets were fitted individually. The scattering length densities of the materials used in this study are listed in Supporting Information, SI1, Table 1. The best fitting of the scattering data from the internal structure of the PLGA-PEG assemblies must not only be physically realistic but also minimize the residuals in the fit.

Fitting to models for simple core−shell particles in water was attempted, but these models did not fit the data; furthermore, the scattering could not be fitted to give realistic SLD values by assuming a solid polymer composite particle surrounded by solvent. Models of a solid PLGA core surrounded by ethylene oxide polymer chains[27] also did not fit the data to give realistic values of the parameters. A model of a fractal structure, composed of polydisperse spherical building blocks, was therefore used to analyze the SANS data from the PLGA-PEG nanoparticles.[28] This model assumes a fractal structure formed from a primary building block of polydisperse PLGA spheres with a radius of R_{avg}, which follows a Schulz distribution. These PLGA blocks were dispersed in a "solvent" of a PEO/water composite forming a network with a fractal geometry.

The form factor of a monodisperse hard sphere is described as

$$P(QR) = \left\{\frac{3[\sin(QR) - QR\cos(QR)]}{(QR)^3}\right\}^2 \quad (3)$$

Where R is the radius of the scattering spherical PLGA building block. The polydispersity in the radius follows a Schulz distribution as[29,30]

$$f(R) = (z+1)^{z+1}x^z\frac{\exp[-(z+1)x]}{R_{avg}\Gamma(z+1)} \quad (4)$$

where R_{avg} is the average PLGA block radius and x is the scaled variable $x = R/R_{avg}$, z is related to polydispersity via $z = 1/p^2 - 1$, and p is the ratio of the standard deviation σ to the average radius as $p = \sigma/R_{avg}$; σ^2 is the variance in the distribution. Finally, substituting in eq 3, the form factor for polydisperse hard spheres is described as

$$P_{poly}(QR) = \phi\Delta\rho^2\left(\frac{4\pi}{3}\right)\int_0^\infty R^3 f(R)P(QR)\,dR \quad (5)$$

The spherical PLGA building blocks aggregate to form fractal-like clusters (PLGA-PEG nanoparticles) in the solvent. The clusters have a correlation length ξ corresponding to their overall size and self-similarity dimension D_f. The interference from PLGA building blocks in a fractal-like cluster can be calculated as[28]

$$S(Q) = 1 + \frac{\sin[(D_f-1)\tan^{-1}(Q\xi)]}{(QR)^{D_f}}\frac{D_f\Gamma(D_f-1)}{[1+1/(Q^2\xi^2)]^{(D_f-1)/2}} \quad (6)$$

The number density of PLGA building blocks is

$$N = \phi/V_p \quad (7)$$

where $V_p = (4/3)\pi(R_{avg})^3$.

The mean number of PLGA blocks per cluster (aggregation number) is

$$G = \Gamma(D_f+1)(\xi/R_{avg})^{D_f} \quad (8)$$

while the radius of gyration of a cluster is

$$R_G^2 = D_f(D_f+1)\xi^2/2 \quad (9)$$

2.2.5. In Vitro Release of Carboplatin from PLGA-PEG Nanoparticles. Nanoparticles (5 mg) were suspended in 0.5 mL of ACSF solution and placed in a centrifuge filter tube (MCOFF 10 K) at 37 °C. At predetermined intervals (refer to Figure 3), samples were centrifuged at 11000 rpm for 15 min, and all ACSF solution was collected and replaced with a fresh aliquot. Finally, the remaining particles were collected, dissolved in 0.6 mL of DCM and vortexed for 3 min. One milliliter of ACSF was then added to the solution, and the mixed solution was then vortexed for 3 min to extract carboplatin into the ACSF solution. This solution was then centrifuged at 11000 rpm for 15 min, and the upper aqueous solution containing the extracted carboplatin was removed by pipet and collected before fresh ACSF solution was replaced onto the DCM solution. The whole extraction process was repeated five times to make sure that any remaining carboplatin in the particles was fully extracted. The carboplatin concentration in the collected solutions was measured by inductively coupled plasma mass spectrometry (Thermo Fisher Scientific XSeries 2 ICP-MS) at the Southampton Oceanography Center, U.K. Iridium (Ir) was used as internal standard. It was expected that, because of its similar mass and ionization potential, the behavior of Ir would accurately reflect that of Pt in that it will have a similar response to matrix effects and possible plasma fluctuations. Quantification was determined against a calibration curve using weighted linear regression analysis.

3. RESULTS AND DISCUSSION

3.1. Synthesis of PLGA-PEG Copolymer. The PLGA-PEG copolymer was synthesized by direct conjugation of PLGA-COOH with NH_2-PEG-CH_3 via the EDC/NHS technique.[8,10] The chemical composition of the synthesized product was confirmed by ^{1}H NMR (Supporting Information, SI2, Figure 1), and the PLGA-PEG number-average molecular weight and polydispersity were measured to be 22 kDa and 1.63, respectively. The molecular weight of the PLGA starting material was 7−17 kDa (as reported by Sigma-Aldrich) and that of the PEG 5.5 kDa (as reported by Polymer Source Inc., Dorval, Canada). The molar ratio of LA monomers/GA monomers/PEG monomers is 1:1:0.08, which was calculated by taking the ratio between the integrated spectrum intensity at 5.2, 4.8, and 3.6 ppm.

3.2. Particle Size, Polydispersity, ζ-Potential, and Morphology Characterization. Particle size is one of the most important parameters that determine the fate of both in vitro and in vivo nanoparticle drug delivery. The nanoparticle diameters determined by DLS were 134, 154, and 186 nm for particles prepared from the same batch of polymer using MeCN, AC, and THF as the water miscible solvents, respectively (Table 1). These measurements were stable when repeated after 1 week.

Previous studies have suggested that the dielectric constant of the solvent, ε, the Hildebrand solubility parameter, δ, and the

DOI: 10.1021/bm501519u
Biomacromolecules 2015, 16, 457−464

interaction parameter, χ (the affinity of the organic solvent for the nonsolvent) can affect the nanoparticle size.[8,31] The interaction parameter χ is expressed as

$$\chi = \frac{V_{NS}}{RT}(\delta_S - \delta_{NS})^2 \quad (10)$$

where V_{NS} is the molar volume of the nonsolvent. The calculated interaction parameters are presented in Table 1. A smaller interaction parameter (increased organic solvent/water affinity) results in a smaller average nanoparticle size, due to more efficient solvent diffusion and polymer dispersion into water.[31] We chose three water-miscible solvents, acetone (AC), acetonitrile (MeCN), and tetrahydrofuran (THF), to prepare PLGA nanoparticles. The standard Hildebrand solubility parameters are 1520, 769, 646, and 588 $kJ^{1/2}$ $m^{-3/2}$ for water[32] (δ_{NS}), MeCN,[33] AC,[34] and THF[35] (δ_S), respectively. The interaction parameters for the solvents increase in the sequence of MeCN < AC < THF; therefore the particle size should be expected to increase in the sequence of MeCN < AC < THF. Light scattering experiment results confirmed the dependence of nanoparticle size on the Hildebrand solubility parameters, as shown in Table 1. The hydrodynamic diameter of PLGA-PEG nanoparticles prepared in a more water-miscible solvent is smaller. The polydispersity of PLGA-PEG nanoparticles is around 0.14, which is higher than that of pure PLGA (RG502H) nanoparticles. Compared with the PLGA nanoparticle, which has a ζ-potential value of −36.9 mV, all the PLGA-PEG nanoparticles exhibited less negative ζ-potential values around −23 mV, consistent with the presence of electroneutral PEG on the particle surface. The variation of organic solvent does not make much difference to the nanoparticle polydispersity and the ζ-potential values.

Table 1. Calculated Interaction Parameter, χ, of Solvent (MeCN, AC, THF)/Nonsolvent (Water) Binary Mixtures and Average Hydrodynamic Diameter (D_{hyd}), Polydispersity (PDI), and ζ-Potential of PLGA-PEG Nanoparticles Prepared with Different Organic Solvents as Determined by Dynamic Light Scattering.

sample	χ^a	D_{hyd} (nm)^b	PDI^b	ζ-potential (mV)^b
PLGA-AC		176 ± 1	0.079 ± 0.010	−36.9 ± 0.6
PLGA-PEG-MeCN	4.09	134 ± 2	0.143 ± 0.007	−22.9 ± 0.6
PLGA-PEG-AC	5.73	154 ± 3	0.149 ± 0.006	−22.6 ± 0.4
PLGA-PEG-THF	6.30	186 ± 4	0.137 ± 0.020	−21.5 ± 0.6

[a]Calculated using eq 10 for T = 25 °C (298 K). [b]Mean ± SD.

TEM images of the PLGA-PEG nanoparticles prepared with different organic solvents are presented in Figure 1. They revealed that the nanoparticles are spherical and that the solvent does not greatly affect the particle morphology. Some of the particles appear deformed, probably due to the sonication of the sample before the deposition of the sample suspension solution on the TEM grid or melting under the electron beam. The average particle radius and the size distribution parameter can be obtained from TEM images using ImageJ software by the fitting of the particle distributions using log-normal distributions. The statistically averaged value of the particle diameter generated from TEM pictures is about 70 ± 10 nm, which is smaller than the results obtained from DLS. TEM measures the dry particle size, while the size obtained from DLS is the hydrodynamic diameter, which includes the hydration shell around the particles.[36−38] The size distribution parameter obtained from TEM images is about 0.19 ± 0.05, which is close to that measured by DLS, showing that the drying process did not induce much change in the size distribution, for example, by aggregating the nanoparticles.

3.3. Internal Structure of PLGA-PEG Nanoparticles.

SANS has been widely used for measuring polymeric micelles or micelle-like nanoparticles prepared with low molecular weight block copolymers. The particle concentration is kept very low in such measurements; therefore the structure factor tends to unity and can be disregarded.[18] In our case, models of polydisperse spheres, solid ellipsoidal PLGA cores with a shell of PEG chains,[27] or core−shell spherical structures were attempted to fit the data but could not successfully fit the data at the low Q range; therefore the structure factor, $S(Q)$, arising from scattering between particles should also be considered in the fitting. However models using standard structure factors for hard spheres or charged spheres also did not provide suitable fits to the data. Instead the scattering suggests that the nanoparticles were formed of fractal aggregates of smaller blocks; therefore, over the Q-range measured, SANS gives detailed information about the internal structure of the PLGA-PEG nanoparticles. Given that this result is distinctly different from an earlier SANS study on similar particles,[18] the experiment was repeated on a second occasion to ensure that the results were reliable.

SANS data sets obtained at two different D_2O/H_2O contrasts were fitted simultaneously to the model described in the Experimental Section, as shown in Figure 2 and Supporting Information, SI3, Figure 2. The scattering length density of the

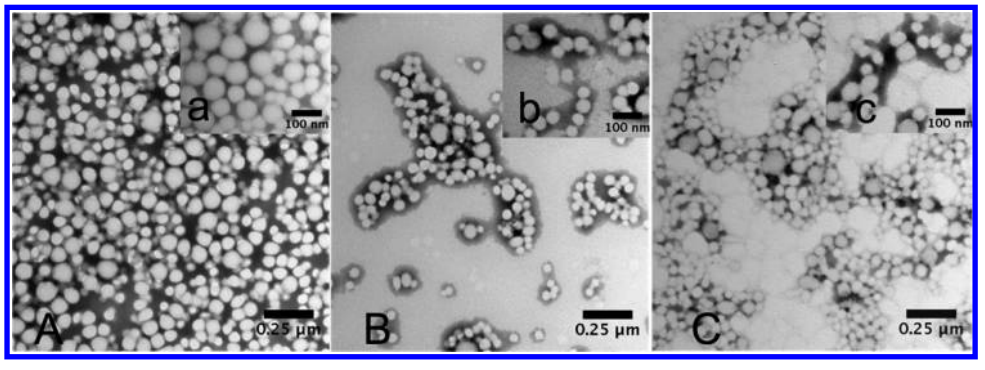

Figure 1. Transmission electron micrographs of PLGA-PEG nanoparticles prepared with different organic solvents: (A) MeCN; (B) THF; (C) AC. All the nanoparticles were negatively stained with phosphotungstic acid solution.

DOI: 10.1021/bm501519u
Biomacromolecules 2015, 16, 457−464

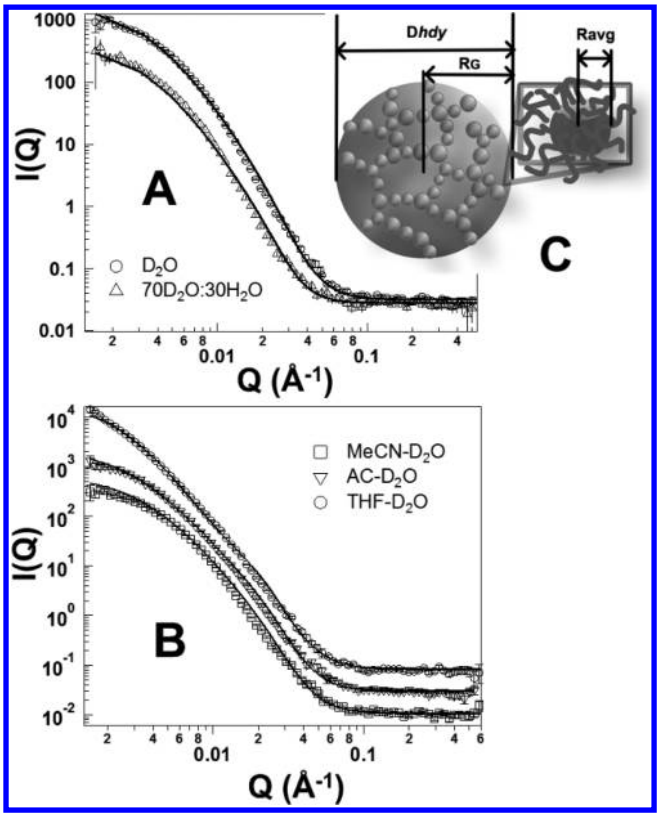

Figure 2. (A) SANS patterns from PLGA-PEG nanoparticles prepared with solvent MeCN at two solvent contrasts (circles, 100% D_2O; triangles, 70% D_2O and 30% H_2O). (B) SANS patterns from PLGA-PEG nanoparticles prepared with different organic solvents: AC, MeCN, and THF in 100% D_2O. The MeCN and THF patterns are vertically offset for clarity, by a factor of 3. The continuous lines are a simultaneous fit to both solvent contrast data sets to the model described in the text. (C) Schematic representation of the internal structure of PLGA-PEG nanoparticle, where polydisperse PLGA blocks are embedded in a PEG/water phase. R_G is the radius of gyration (note this is approximate; R_G is the root-mean-square distance of the parts of an object from its center of mass), D_{hyd} is the hydrodynamic diameter of the whole PLGA-PEG nanoparticle, and R_{avg} is the average radius of PLGA block within the particle).

PLGA building block was set at the calculated value 2.10×10^{-6} $Å^{-2}$ assuming that no water penetrates into PLGA blocks (Supporting Information, SI2, Table 1). Five variables were allowed to fit during the data-fitting process (PLGA block radius, fractal dimension, PLGA block polydispersity, correlation length, and "solvent SLD" composed of a PEG/water mixture). The aggregation number, G, and radius of gyration, R_G, of the whole PLGA-PEG−water cluster were calculated using eqs 8 and 9, respectively. The volume fraction (ϕ) of PLGA blocks inside a cluster was calculated using $V_pG/V_{cluster}$. The scattering length density of the "solvent" depends on the volume fraction of PEG (φ_{PEG}) and water (φ_{water}) (φ_{PEG} + φ_{water} = 1). φ_{PEG} was obtained by calculation using the two solvent SLD values at different D_2O/H_2O contrasts and that of PEO. Nanoparticles prepared using PLGA-PEG block copolymers from two different synthesis batches were used for the two separate neutron scattering experiments (D11 at ILL and SANS2D at ISIS), respectively. All fitted and calculated parameters of the SANS data collected from SANS2D, ISIS, are shown in Table 2, while the fitted and calculated parameters of the SANS data collected from D11, ILL, are shown in Supporting Information, SI4, Figure 3, and SI5, Table 2; for the D11 experiment, only 100% D_2O was used as a solvent. The fitted parameters did not reach lower or upper bound limits during the minimization process. The good agreement of the two sets of results indicates good experimental reproducibility.

Table 2. Values of Parameters Obtained from a Simultaneous Analysis of the Multicontrast SANS Data Obtained from PLGA-PEG Nanoparticles Using the Model Described in the Text[a]

	solvent		
	MeCN	AC	THF
Fitted Parameters			
PLGA block radius, R_{avg} (nm, ±0.5 nm)	7.5	7.8	9.0
fractal dimension, D_f (±0.01)	2.63	2.68	2.98
PLGA block polydispersity, z (±0.02)	0.46	0.39	0.37
correlation length, ξ (nm, ±0.1 nm)	30.0	33.6	40.0
ρ_{PEG+D_2O} ($\times 10^{-6}$ $Å^{-2}$, $\pm 10^{-8}$ $Å^{-2}$)	2.34	2.32	2.28
$\rho_{PEG+70D_2O/30H_2O}$ ($\times 10^{-6}$ $Å^{-2}$, $\pm 10^{-8}$ $Å^{-2}$)	2.21	1.98	2.18
Calculated Parameters			
volume fraction, ϕ (±0.05)	0.21	0.22	0.40
aggregation number, G (±25)	148	202	512
radius of gyration of cluster, R_G (nm, ±0.6 nm)	65.7	74.7	97.7
PLGA block volume, V_p ($\times 10^5$, nm^3)	2.62	4.10	15.7
$V_{PEG+water}$ ($\times 10^5$, nm^3)	9.25	13.4	23.4
volume fraction PEG, φ_{PEG}	0.93	0.83	0.95
$S_{PLGA-PEG}$ ($\times 10^5$, nm^2)	1.04	1.56	5.22

[a]The actual fittings are shown graphically in Figure 2 and Supporting Information, SI3, Figure 2. ρ_{PEG+D_2O} = SLD of solvent composed of PEG/100% D_2O; $\rho_{PEG+70D_2O/30H_2O}$ = SLD of solvent composed of PEG/70% D_2O and 30% H_2O; R_G = radius of gyration of whole PLGA-PEG−water cluster; $V_{PEG+water}$ = volume of PEG/water region in the cluster; the volume fraction (ϕ) of PLGA blocks inside a cluster was calculated from $V_pG/V_{cluster}$; φ_{PEG} = volume fraction of PEG in the water phase, $S_{PLGA-PEG}$ = PLGA-PEG surface area.

The fitting results indicate that the average radius of the small PLGA building blocks increases from 7.5 to 9 nm while the polydispersity of the PLGA blocks decreases from 0.46 to 0.37 as the solvents used to make the particles become less miscible with water in the sequence of MeCN, AC, and THF. Less miscible solvents result in less efficient solvent diffusion and polymer dispersion, allowing more time for the PLGA-PEG polymer to fuse into bigger aggregates with smaller polydispersity values.

The entire phase diagram for PLA-PEO copolymers in water as a function of the PLA fraction in the copolymer was calculated using atomistic molecular dynamics simulations by Posocco.[39] When the copolymer concentration in water was less than 20% v/v, only micelles were observed for the entire range of PLA fraction (from 0 to 1). When the PLA fraction is much higher than the PEO fraction, crew-cut micelles with large insoluble blocks in the core and short soluble blocks in the coronas are the dominant morphology. In this study, the starting copolymer concentration is 0.27% v/v and PLGA molar fraction is 0.93, so a micellar form should be the preferable morphology in the copolymer/water systems, although much larger particles are observed in our system. Interestingly, the radius of the PLGA blocks in our particles is about 7.5−9 nm, which is only slightly smaller than that of the PLA core (11 nm) found for core−shell particles prepared from acetone using PLGA-PEG with a 15.6/5 kDa ratio by Riley et

DOI: 10.1021/bm501519u
Biomacromolecules 2015, 16, 457−464

al.[18] This corresponds to the slightly smaller PLGA molecular weight (average MW is 14 kDa, measured by GPC) used here.[18] For PLGA-PEG nanoparticles prepared with acetone in our work, the correlation distance between blocks is about 30 nm; thus the spacing between the PLGA blocks is about 14 nm, which is twice the size of PEG layer thickness of the PLGA-PEG block. This result is similar to the PEG shell thickness (6.7 nm) described by Riley.[18] This suggests that the larger particles prepared here could be formed by aggregation of initially formed small core−shell micelles during the synthesis process caused by the higher concentrations used in this work (3.33 mg/mL compared with 0.7 mg/mL in the study by Riley et al.[18]). The number density of building blocks was calculated from the model to give a mean number of blocks per cluster and radius of gyration of the cluster.[28] The mean block number increased from 148 to 512, and the cluster radius of gyration increased from 66 to 98 nm as the organic/water solvent miscibility decreased. The calculated radius of gyration results are in agreement with the hydrodynamic radii measured from DLS. The volume of PLGA polymer is calculated from the PLGA block radius, and it increased from 2.62×10^5 to 15.7×10^5 nm^3 as the organic/water miscibility decreased. Overall, these results describe a trend of a smaller PLGA block, higher block polydispersity, and smaller radius of gyration (nanoparticle size) when the organic solvent/water miscibility used in the nanoparticle preparation increases.

The calculated PEG volume fractions in the water/PEG regions of the particle are 0.93, 0.83, and 0.95 for particles prepared with MeCN, AC, and THF, respectively. These high volume fractions of PEG suggest why the internal structure cannot be seen in the TEM images, since the density of this phase will be very similar to that of the PLGA fraction (50:50 PLGA has a density of 1.34 g/cm^3, while a 50 wt % PEG solution in water is 1.1 g/cm^3,[40] and the PEG volume fractions here are even higher). Using the volume fractions and the other SANS results in Table 2, we can calculate the dry volume of the particles. As an example, considering the particles precipitated using acetone, if only PEG remains in the PEG/water regions when the particles are dry, the volume of this region will be $0.83 \times 13.4 \times 10^5$ nm^3, while the PLGA block volume in the particle is 4.10×10^5 nm^3. Thus the total dry nanoparticle volume will be $\sim 15.2 \times 10^5$ nm^3, giving a nanoparticle diameter of about 71 nm, which is very close to the particle diameter observed by TEM (Figure 1 above).

The mass-fractal dimension, which has physically acceptable values between 1 and 3, describes how the cluster mass spatially scales with the cluster size and depends on the process for the cluster growth. Values less than 3 suggest that the structure is more open than a completely compact three-dimensional collapsed polymer,[41] while values around 1.8 suggest formation of diffusion limited aggregates. The values in this case are well over 2 (MeCN 2.63; AC 2.68; THF 2.98), suggesting that the aggregates are relatively densely packed, with the structure arising from reaction-limited aggregation.[42] This supports the idea that the larger particles are formed from the rapid aggregation of smaller micelle-like species during the nanoprecipitation process.

3.4. In Vitro Carboplatin Release from the PLGA-PEG Nanoparticles. Efficient use of drugs requires their selective delivery to the site of action at a controlled rate. Carboplatin is clinically used in anticancer chemotherapy and is associated with severe side effects because of poor specificity.[43,44] The selective delivery of carboplatin to tumor cells would significantly reduce drug toxicity and avoid damage to normal tissues. One strategy involved local administration of the platinum-based drug to easily accessible tumors as a water soluble drug−polymer complex. Alternately, improved tumor targeting has also been achieved using colloidal platinum drug loaded carriers, such as polymeric micelles, exhibiting prolonged blood residence and a reduction of toxicity after administration.[44] In this work, we investigated the feasibility of loading carboplatin into the PLGA-PEG nanoparticles. The in vitro drug release profiles were obtained and are compared with the internal structure of PLGA-PEG nanoparticles investigated using SANS techniques.

Carboplatin was successfully encapsulated inside the PLGA-PEG nanoparticles. The drug loading and in vitro release profiles were evaluated using ICP-MS (Figure 3). The drug loading efficiency is low due to the high water solubility of carboplatin (15 mg/mL);[43] however it is sufficient for determining release profiles from the particles. PLGA-PEG nanoparticles prepared with acetone had a relatively higher drug loading (0.41%) compared with the nanoparticles prepared with MeCN and THF (0.1−0.2% drug loading). Similar loadings have also been obtained with cisplatin, which is physically trapped using PLGA-PEG nanoparticles.[6] Carboplatin is more likely to associate with the PEG/water network or to sit near the surface between PLGA and PEG due to its hydrophilicity. The difference in drug loading between particles prepared from different initial solvents may therefore be due to two reasons: (1) variation in the PLGA-PEG surface area or PEG volume, as shown in Table 2; (2) organic solvent miscibility with water. THF is less miscible with water; therefore particle precipitation is delayed, so the water soluble drug has a longer time to leak out of the PEG network during the preparation process. Both of these factors play a role, so particles prepared from THF have higher surface area but less drug loading, while particles prepared from acetone have an intermediate surface area but the miscibility of acetone with water limits drug loss during particle formation.

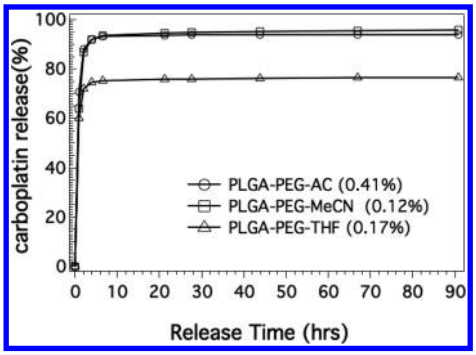

Figure 3. In vitro carboplatin release from PLGA-PEG nanoparticles prepared using different organic solvents: AC (circle), MeCN (square), and THF (triangle) in ACSF solution. The drug loading value is shown inside the parentheses.

The release of carboplatin from the nanoparticles involved an initial burst release phase, which is followed by a period of relatively slow release. Ninety percent of loaded drug was released in the first 10 h for PLGA-PEG samples prepared with acetone and MeCN, indicating that most of the loaded carboplatin is absorbed on or close to the surface of the nanoparticle and easily escapes. Within the range investigated here, the drug loading did not appear to affect the rate of

DOI: 10.1021/bm501519u
Biomacromolecules 2015, 16, 457−464

carboplatin release from the nanoparticles, which has also been reported by Avgoustakis et al.[6]

The release profile of PLGA-PEG particles prepared with THF indicates that 24% of the encapsulated carboplatin was entrapped in the nanoparticles, and this particle significantly retarded carboplatin in vitro release. In the case of nanoparticles prepared with THF, the SANS data indicates that these particles have the highest PLGA block aggregation number and largest PLGA block size compared with particles prepared with the other two solvents. The larger core-forming block has stronger influence on the PEG layer around it, the number of attractive hydrophobic interactions leads to a tight association between the PLGA chains, and the PLGA chains more forcibly draw together the solvated PEO blocks, having correspondingly more condensed PEG layers.[18,39] The PEG volume fraction of particles prepared with THF (φ_{PEG}), which is calculated from the SLDs of two solvent contrasts to be 0.95, is higher than the PEG volume fraction of the nanoparticles prepared with the MeCN and AC. The higher PEG proportion in the solvent and thick PEG layers as well as the more tightly packed building blocks could retard the drug dissolution in the water and thus slow the drug release from the nanoparticle. Particles prepared with AC have a relative high drug loading; however, they have a low PEG volume fraction of 0.83; therefore, carboplatin easily diffused out from the particle during the in vitro drug release process, resulting in a low retention of carboplatin.

4. CONCLUSIONS

Understanding the internal structures formed within the particles is fundamentally important to explain the difference in drug loading and variations in drug release rate from polymer nanoparticles. In this work, we prepared nanoparticles from synthesized poly(lactide-*co*-glycolide)-*block*-poly(ethylene glycol) (PLGA-PEG-CH_3) polymer via a nanoprecipitation method using three organic solvents (THF, acetone, and acetonitrile) with different solvent/water miscibility. PLGA-PEG nanoparticles were characterized with regards to their size, size distribution, and ζ-potential by DLS and morphology by TEM. Small angle neutron scattering measurements and fitted models revealed the internal nanoparticle structure: PLGA blocks of 7−9 nm are encapsulated inside fairly condensed PEG/water networks in a fractal geometry. Particles prepared with a more water miscible solvent and having a large PLGA-PEG surface area have higher drug loading. Denser particles with larger hydrophobic blocks draw together the PEG blocks, leading to condensed PEG blocks with high PEG volume fraction in the PEG/water phase, resulting in a more controllable hydrophilic anticancer drug carboplatin release profile.

■ ASSOCIATED CONTENT

Supporting Information

^{1}H NMR data for synthesized PLGA-PEG polymers, calculated scattering length densities for different components in the suspensions and fitted SANS patterns for PLGA-PEG nanoparticles prepared with different organic solvents (MeCN, AC, and THF) at 100% D_2O and 70% D_2O contrasts, graphs of fitted patterns for SANS patterns from different experiments, and table of fit parameters for the second experiment. This material is available free of charge via the Internet at http://pubs.acs.org.

■ AUTHOR INFORMATION

Corresponding Author

*Tel +44(0)1225384192, fax +44(0)1225386231, e-mail k.edler@bath.ac.uk.

Present Address

§B.Y.: School of Physics & Astronomy, The University of Nottingham, University Park, Nottingham NG7 2RH, U.K.

Author Contributions

The manuscript was written through contributions of all authors. All authors have given approval to the final version of the manuscript.

Notes

The authors declare no competing financial interest.

■ ACKNOWLEDGMENTS

This work was funded by the UK Medical Research Council (MRC) Grant Number MR/J005134/1. We thank Dr. Ann Terry, Dr. Sarah Rogers (ISIS), and Mr Gavin Hazell for assistance with SANS experiments (XB1293033) on SANS2D, ISIS, U.K., the Institut Laue-Langevin (ILL) for award of beamtime for the SANS experiments (no. 9-11-1611) on instrument D11, Dr. Matthew Jones for help with GPC instrument, Mrs Ursula Potter and Dr. John Mitchels for assistance with TEM, and Dr. Matthew Cooper and Dr. Andy Milton (Ocean and Earth Science, National Oceanography Centre Southampton, University of Southampton) for help with the ICP-MS measurements.

■ REFERENCES

(1) Patel, T.; Zhou, J. B.; Piepmeier, J. M.; Saltzman, W. M. *Adv. Drug Delivery Rev.* **2012**, *64*, 701−705.

(2) Danhier, F.; Ansorena, E.; Silva, J. M.; Coco, R.; Le Breton, A.; Preat, V. *J. Controlled Release* **2012**, *161*, 505−522.

(3) Hans, M. L.; Lowman, A. M. *Curr. Opin. Solid State Mater. Sci.* **2002**, *6*, 319−327.

(4) Dinarvand, R.; Sepehri, N.; Manoochehri, S.; Rouhani, H.; Atyabi, F. *Int. J. Nanomed.* **2011**, *6*, 877−895.

(5) Yoo, J. W.; Chambers, E.; Mitragotri, S. *Curr. Pharm. Des.* **2010**, *16*, 2298−2307.

(6) Avgoustakis, K.; Beletsi, A.; Panagi, Z.; Klepetsanis, P.; Karydas, A. G.; Ithakissios, D. S. *J. Controlled Release* **2002**, *79*, 123−135.

(7) Gryparis, E. C.; Hatziapostolou, M.; Papadimitriou, E.; Avgoustakis, K. *Eur. J. Pharm. Biopharm.* **2007**, *67*, 1−8.

(8) Cheng, J.; Teply, B. A.; Sherifi, I.; Sung, J.; Luther, G.; Gu, F. X.; Levy-Nissenbaum, E.; Radovic-Moreno, A. F.; Langer, R.; Farokhzad, O. C. *Biomaterials* **2007**, *28*, 869−876.

(9) Guo, J. W.; Gao, X. L.; Su, L. N.; Xia, H. M.; Gu, G. Z.; Pang, Z. Q.; Jiang, X. G.; Yao, L.; Chen, J.; Chen, H. Z. *Biomaterials* **2011**, *32*, 8010−8020.

(10) Farokhzad, O. C.; Cheng, J. J.; Teply, B. A.; Sherifi, I.; Jon, S.; Kantoff, P. W.; Richie, J. P.; Langer, R. *Proc. Natl. Acad. Sci. U.S.A.* **2006**, *103*, 6315−6320.

(11) Riley, T.; Stolnik, S.; Heald, C. R.; Xiong, C. D.; Garnett, M. C.; Illum, L.; Davis, S. S.; Purkiss, S. C.; Barlow, R. J.; Gellert, P. R. *Langmuir* **2001**, *17*, 3168−3174.

(12) Govender, T.; Riley, T.; Ehtezazi, T.; Garnett, M. C.; Stolnik, S.; Illum, L.; Davis, S. S. *Int. J. Pharm.* **2000**, *199*, 95−110.

(13) Pierri, E.; Avgoustakis, K. *J. Biomed. Mater. Res., Part A* **2005**, *75A*, 639−647.

(14) Tanodekaew, S.; Pannu, R.; Heatley, F.; Attwood, D.; Booth, C. *Macromol. Chem. Phys.* **1997**, *198*, 927−944.

(15) Hagan, S. A.; Coombes, A. G. A.; Garnett, M. C.; Dunn, S. E.; Davis, M. C.; Illum, L.; Davis, S. S.; Harding, S. E.; Purkiss, S.; Gellert, P. R. *Langmuir* **1996**, *12*, 2153−2161.

DOI: 10.1021/bm501519u
Biomacromolecules 2015, 16, 457−464

(16) Stolnik, S.; Heald, C. R.; Neal, J.; Garnett, M. C.; Davis, S. S.; Illum, L.; Purkis, S. C.; Barlow, R. J.; Gellert, P. R. *J. Drug Target* **2001**, *9*, 361−378.
(17) Heald, C. R.; Stolnik, S.; Kujawinski, K. S.; De Matteis, C.; Garnett, M. C.; Illum, L.; Davis, S. S.; Purkiss, S. C.; Barlow, R. J.; Gellert, P. R. *Langmuir* **2002**, *18*, 3669−3675.
(18) Riley, T.; Heald, C. R.; Stolnik, S.; Garnett, M. C.; Illum, L.; Davis, S. S.; King, S. M.; Heenan, R. K.; Purkiss, S. C.; Barlow, R. J.; Gellert, P. R.; Washington, C. *Langmuir* **2003**, *19*, 8428−8435.
(19) Musumeci, T.; Vicari, L.; Ventura, C. A.; Gulisano, M.; Pignatello, R.; Puglisi, G. *J. Nanosci. Nanotechnol.* **2006**, *6*, 3118−3125.
(20) Vandamme, H.; Levitz, P.; Bergaya, F.; Alcover, J. F.; Gatineau, L.; Fripiat, J. J. *J. Chem. Phys.* **1986**, *85*, 616−625.
(21) Wang, Q.; Liu, P. F.; Gong, T.; Sun, X.; Duan, Y. R.; Zhang, Z. R. *J. Biomed. Nanotechnol.* **2014**, *10*, 993−1003.
(22) Lieutenant, K.; Lindner, P.; Gahler, R. *J. Appl. Crystallogr.* **2007**, *40*, 1056−1063.
(23) Schmatz, W.; Springer, T.; Schelten, J.; Ibel, K. *J. Appl. Crystallogr.* **1974**, *7*, 96−116.
(24) Heenan, R.; King, S.; Turner, D.; Treadgold, J. *Proc ICANS-XVII* **2006**, 780−785.
(25) Heenan, R. K.; Rogers, S. E.; Turner, D.; Terry, A. E.; Treadgold, J.; King, S. M. *Neutron News* **2011**, *22*, 19−21.
(26) Kline, S. R. *J. Appl. Crystallogr.* **2006**, *39*, 895−900.
(27) Pedersen, J. S.; Hamley, I. W.; Ryu, C. Y.; Lodge, T. P. *Macromolecules* **2000**, *33*, 542−550.
(28) Teixeira, J. *J. Appl. Crystallogr.* **1988**, *21*, 781−785.
(29) Kotlarchyk, M.; Chen, S. H. *J. Chem. Phys.* **1983**, *79*, 2461−2469.
(30) Schulz, G. V. *Z. Phys. Chem.* **1935**, *43*, 25.
(31) Bilati, U.; Allemann, E.; Doelker, E. *Eur. J. Pharm. Sci.* **2005**, *24*, 67−75.
(32) Burke, J. Book and Paper Group Annual 1984, Vol. 3, http://cool.conservation-us.org/coolaic/sg/bpg/annual/v03/bp03-04.html, (accessed 12/21/2014).
(33) Stenutz, R. http://www.stenutz.eu/chem/solv6.php?name=acetonitrile, (accessed 12/21/2014).
(34) Stenutz, R. http://www.stenutz.eu/chem/solv6.php?name=acetone, (accessed 12/21/2014).
(35) Stenutz, R. http://www.stenutz.eu/chem/solv6.php?name=tetrahydrofuran, (accessed 12/21/2014).
(36) Cooper, D. L.; Harirforoosh, S. *PLoS One* **2014**, *9*, No. e87326.
(37) Raemdonck, K.; Braeckmans, K.; Demeester, J.; De Smedt, S. C. *Chem. Soc. Rev.* **2014**, *43*, 444−472.
(38) Gaumet, M.; Vargas, A.; Gurny, R.; Delie, F. *Eur. J. Pharm. Biopharm.* **2008**, *69*, 1−9.
(39) Posocco, P.; Fermeglia, M.; Pricl, S. *J. Mater. Chem.* **2010**, *20*, 7742−7753.
(40) Gonzalez-Tello, P.; Camacho, F.; Blazquez, G. *J. Chem. Eng. Data* **1994**, *39*, 611−614.
(41) Enright, M. B.; Leitner, D. M. *Phys. Rev. E* **2005**, *71*, No. 011912.
(42) Weitz, D. A.; Huang, J. S.; Lin, M. Y.; Sung, J. *Phys. Rev. Lett.* **1985**, *54*, 1416−1419.
(43) Haxton, K. J.; Burt, H. M. *J. Pharm. Sci.* **2009**, *98*, 2299−2316.
(44) Wang, X. Y.; Guo, Z. J. *Chem. Soc. Rev.* **2013**, *42*, 202−224.

DOI: 10.1021/bm501519u
Biomacromolecules 2015, 16, 457−464